*Chem Biol Drug Des 2015*; **86:** 546–558

Research Article

# Estimation of the Binding Free Energy of AC1NX476 to HIV-1 Protease Wild Type and Mutations Using Free Energy Perturbation Method

**Son Tung Ngo[1,2,*], Binh Khanh Mai[3], Dinh Minh Hiep[4] and Mai Suan Li[2,*]**

[1]*Institute for Computational Science and Technology, Quang Trung Software City, Tan Chanh Hiep Ward, District 12, Ho Chi Minh City, Vietnam*
[2]*Institute of Physics, Polish Academy of Sciences, Al. Lotnikow 32/46, 02-668 Warsaw, Poland*
[3]*Department of Applied Chemistry, College of Applied Sciences, Kyung Hee University, Yongin 446-701, Korea*
[4]*Department of Sciences and Technology, 244 Dien Bien Phu Street , Ward 7, District 3,,Ho Chi Minh City, Vietnam*
**Corresponding authors: Son Tung Ngo, nstung@ifpan.edu.pl; Mai Suan Li, masli@ifpan.edu.pl*

**The binding mechanism of AC1NX476 to HIV-1 protease wild type and mutations was studied by the docking and molecular dynamics simulations. The binding free energy was calculated using the double-annihilation binding free energy method. It is shown that the binding affinity of AC1NX476 to wild type is higher than not only ritonavir but also darunavir, making AC1NX476 become attractive candidate for HIV treatment. Our theoretical results are in excellent agreement with the experimental data as the correlation coefficient between calculated and experimentally measured binding free energies $R = 0.993$. Residues Asp25-A, Asp29-A, Asp30-A, Ile47-A, Gly48-A, and Val50-A from chain A, and Asp25-B from chain B play a crucial role in the ligand binding. The mutations were found to reduce the receptor–ligand interaction by widening the binding cavity, and the binding propensity is mainly driven by the van der Waals interaction. Our finding may be useful for designing potential drugs to combat with HIV.**

**Key words:** AC1NX476, binding cavity, binding free energy, darunavir, docking, free energy perturbation method, HIV-1 protease, ritonavir

Received 15 October 2014, revised 16 December 2014 and accepted for publication 5 January 2015

The human immunodeficiency virus (HIV), which is the cause of acquired immunodeficiency syndrome (AIDS), currently infects approximately 34 million people around the world. Nearly 30 million people have died of AIDS-related causes from the beginning of the epidemic (1–3). HIV-1 protease (HIV-1 PR) is an essential enzyme in the life cycle of HIV for the protein maturation and viral infection (4). This is the reason why it has become one of the most popular targets in the structure-based drug design. The licensed drugs available for HIV-1 PR include saquinavir, ritonavir, indinavir, nelfinavir, amprenavir, and lopinavir (5).

After the discovery of HIV-1 PR inhibitors, powerful reverse transcriptase inhibitors have also been introduced into the clinical practice (6). However, protease inactivation remains a fundamental therapeutic tool, and new HIV-1 PR inhibitors, such as darunavir (7), become available after 2005 and are currently used in association with reverse transcriptase inhibitors. Moreover, the proficiency of HIV-1 PR-based therapies is limited in time due to the occurrence of drug-resistant mutant viral strains (8,9) and severe side-effects. Therefore, the development of new inhibitors that are efficient for both wild type and its mutations is still an object of intense research.

The binding affinity of ligands to HIV-1 PR has been intensively studied by molecular dynamics (MD) simulations (10–13). The double-decoupling free energy simulation method (14) was used to estimate the contribution to the binding free energy from interfacial water molecules resided in the crystal structure of HIV-1 protease in complex with potent inhibitor Kynostatin 272 (KNI-272) (15). The interaction of ritonavir (16) and darunavir (17) with HIV-1 PR has been investigated using the MM-PBSA method (18). This method in combination with quantum mechanical calculations indicated the importance of the stability of HIV-1 PR flaps toward binding of darunavir (19). A comparative study of saquinavir complexed with wild-type HIV-1 PR and single mutants was carried out by Tzoupis and coworkers (20) using MD, MM-PBSA, and thermodynamic integration approaches. Recently, the computation of binding free energies of some HIV-1 PR inhibitors, which may be clinically relevant, has been performed by a combination of MM-PBSA and MM-GBSA methods (12).

The compound AC1NX476, which is also known as brecanavir analog 5, is a small molecule discovered by



 doi: 10.1111/cbdd.12518

Hanlon *et al.* (21). The experiment showed that it can block HIV-1 PR wild-type (WT) activity with inhibition constant $K_i$ = 6 fM (21), which corresponds to the binding free energy $\triangle G_{exp}$ = −19.54 kcal/mol. AC1NX476 also has the high binding affinity to HIV-1 PR mutation 1 (I50V), mutation 2 (M26I, L63P, A71V, V82F, and I84V), and mutation 3 (L10I, L19Q, K20R, E35D, M36I, S37N, M46I, I50V, I54V, I62V, L63P, A71V, V82A, and L90M) with $\triangle G_{exp}$ = −15.92, −16.17 and −17.01 kcal/mol (21), respectively. In what follows, the mutations 1, 2, and 3 will be referred to as MT1, MT2, and MT3. Note that the binding free energy of ritonavir to WT $\triangle G_{exp}$ = −14.70 kcal/mol) (22), currently used for treatment of HIV/AIDS, is smaller in magnitude than that of AC1NX476 to HIV-1 PR sequences. Therefore, AC1NX476 would be a good inhibitor not only for WT, but also for its mutations.

Despite a potential importance of AC1NX476 for HIV treatment, its binding mechanism to HIV-1 PR variants has not been studied theoretically. The goal of this study was to estimate the binding free energy of AC1NX476 to HIV-1 PR WT and mutations and to understand the main factors governing its binding affinity. The knowledge about such factors would considerably save our time to search for potential drugs for HIV/AIDS.

The binding properties of AC1NX476 to HIV-1 PR variants were first analyzed by the molecular docking method. As this method is not accurate enough, the binding free energy was further refined using the free energy perturbation (FEP) method (23). For comparison with AC1NX476, we have also studied the binding of ritonavir and darunavir to HIV-1 PR WT by the same FEP method. It is shown that, in agreement with the experiments, the ranking of binding affinity of AC1NX476 to HIV-1 PR sequences is WT > MT2 > MT3 > MT1. Moreover, the correlation between experimental and theoretical values of $\triangle G_{bind}$ is very high implying that the FEP method is a useful tool for studying ligand binding to proteins. The van der Waals (vdW) interaction was found to dominate over the electrostatic interaction, but electronegative atoms of ligand are prominent in blocking activity of HIV-1 PR. Residues Asp25-A, Asp29-A, Asp30-A, Ile47-A, Gly48-A, **Val50-A**, and Asp25-B in the binding site play a key role in AC1NX476 binding (hereafter, mutated residues will be highlighted by bold font). One can show that the binding free energy depends on the number of non-bonded water molecules interacting with the ligand and the volume of binding cavity.

## Methods and Materials

### *Crystal structure of receptors and ligands*

The two-dimensional plot of AC1NX476 ($C_{34}H_{41}N_3O_{10}S$) is shown in Figure 1, while its 89 atoms are presented in Figure S1. The three-dimensional structure of this compound was built and optimized with the help of Gabedit-2.4.6 software (24). HIV-1 PR has two chains A and B spanning residues Pro1-A–Asn99-A and Pro1-B–Asn99-B, respectively.

The starting structure of HIV-1 PR WT with bound ritonavir was taken from the Protein Data Bank (PDB) [PDB ID: 1HXW (25)]. The 2D structure of ritonavir is shown in Figure S2. The darunavir bound to WT at two different positions will be referred to as darunavir 1 and darunavir 2, and the corresponding structures were taken from PDB [PDB ID: 4LL3 (26)]. The 2D structure of darunavir is shown in Figure S2. The X-ray diffraction structure of MT1 was also taken from PDB [PDB ID: 2R3T (27)]. Because the atomic structure of MT2 is currently unavailable, we used the closest structure of HIV-1 PR mutation (K20R, V32I, L33F, M46I, L63P, A71V, V82A, I84V, and L90M in chain A) with PDB ID 2B7Z to generate its structure by the mutagenesis module in the PYMOL package (28–30). Finally, the structure of MT3 was taken from PDB [PDB ID: 2FDD (31)].

Because structures of all sequences complexed with AC1NX476 are not available in the PDB, they were obtained by docking AC1NX476 to PDB structures 1HXW, 2R3T, 2B7Z, and 2FDD for WT, MT1, MT2, and MT3, respectively. The list of all structures used in our simulations is given in Table S1, while their plots are shown in Figure 1 and Figure S3.

As the protonation state of residues Asp25-A and Asp25-B may significantly affect the ligand binding (32), we consider this problem in detail. In the WT+ritonavir case,

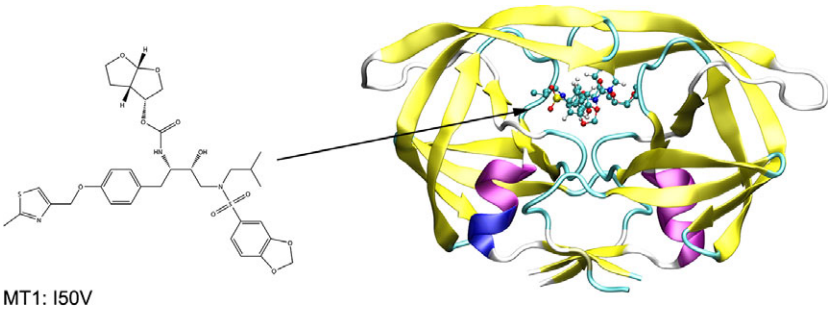


**Figure 1:** Chemical structure of AC1NX476 (left) and the equilibrium structure of solvated complex WT+AC1NX476 (right). Shown are four receptors WT, MT1, MT2, and MT3 used in theoretical calculations.

Asp25-A is protonated, while Asp25-B is deprotonated (16). Aspartic acid residues of the active site were modeled in protonated state for the WT+darunavir complex, according to previous experimental and theoretical studies (33–35). Because neither experimental nor theoretical information on protonation state of Asp25-A and Asp25-B is available for complexes with AC1NX476, the PROPKA server (36–39) was used to analyze the protonation state of both residues. As in the case of WT+ritonavir, for all sequences, Asp25-A is protonated with deprotonation of Asp25-B.

In our simulations, Asp29, Asp30, Asp60, Glu21, Glu34, Glu35, Glu65, and His69 in both chains are deprotonated, while Lys14, Lys20, Lys43, Lys45, Lys55, Lys70, Arg8, Arg41, and Arg57 from chain A and B are protonated. This information was also obtained by the PROPKA server.

### Docking method

Starting structures of receptor–ligand complexes were generated using Autodock Tools 1.5.4 (40). AUTODOCK VINA version 1.1 (41) was employed to dock AC1NX476 to WT and mutations. This docking method uses the idea of empirical scoring (42,43) that the total binding energy can be separated into several physically distinct contributions. The Broyden–Fletcher–Goldfarb–Shanno method (44) was implemented for local optimization, while the atomic interactions were described by the modified version of CHARMM force field (45,46). The maximum energy difference between the best and worst binding modes was chosen to be 7 kcal/mol. Twenty binding modes were generated with random positions of a ligand that has fully flexible torsion degrees of freedom, but the receptor flexibility is not allowed. The center of grids was placed at the center of binding site, and grid dimensions were chosen large enough (24 × 26 × 40 Å) to cover the entire binding site of receptor.

### Molecular dynamics simulations

For those complexes the holo-structures of which are available in PDB, we used the PDB structures as starting configurations for molecular dynamics (MD) simulations. Thus, the PDB structure [PDB ID: 1HXW (25)] was used for the WT+ritonavir, while the structure with PDB ID 4LL3 (26) was used for WT+darunavir 1 and WT+darunavir 2 (Table S1). Recall that darunavir 1 and 2 refer to complexes with darunavir in position 1 and position 2, respectively. Because holo-structures of complexes of AC1NX476 with HIV-1 PR variants are not available in PDB, the lowest binding energy configurations, obtained by the docking method, were used as the starting configurations for MD runs (Table S1). The initial structures of all complexes are shown in Figure S3.

We have also performed MD simulations for AC1NX476, ritonavir, and darunavir in solvent for the double-annihilation binding free energy analysis. The GROMACS 4.5.5 package (47) was utilized to run MD simulations with the Gromos96 43a1 force field (48,49) and SPC water model (50) because this water model is the most suitable partner for Gromos96 force field in studying the protein–ligand interaction (51). The PRODRG2 Beta server (52) was used to generate topology parameters for AC1NX476 and ritonavir. As charges assigned by this server (52) provide unrealistic partitioning between water and cyclohexane phases (53), we used restrained electrostatic potential (RESP) method (54) to estimate charges at the Hartree–Fock (HF)/6-31G(d) level in the gas phase.

The accurate leapfrog stochastic dynamics integrator was employed for MD simulations (55) at 300 K with a relaxation time of 0.1 ps at 1.0 atm and the Parrinello-Rahman pressure control (56). We used LINCS (57) with order 8 to constrain only the bonds involving hydrogen atoms, and the time step 2 fs was chosen. The fast smooth particle-mesh Ewald electrostatics (PME) method (58) was employed to compute the electrostatic interaction. The cutoff of the Lennard-Jones interaction was set equal 0.9 nm, while the non-bonded interaction pair list with a cutoff of 1.0 nm was updated every 10 fs. The dodecahedron boxes with periodic boundary conditions contained more than 10 000 and 900 water molecules for complex and ligand in solvent, respectively. Counter ions Na+ have been added to neutralize the system.

By carrying out three energy minimization steps with the steepest decent, conjugate gradient, and low-memory Broyden–Fletcher–Goldfarb–Shanno method (44), the solvated complex and ligand systems were first minimized until the maximum force became smaller than $2 \times 10^{-6}$ kJ/(mol nm) for the solvated complex and $10^{-6}$ kJ/(mol nm) for the solvated ligand. We applied a weak restrained force for solvated systems using harmonic potential and performed constant temperature MD simulations for 100 ps. To reach equilibrium, we have performed simulations of 20 ns for the solvated complexes and 2 ns for solvated ligands. The last snapshots will be used for further MD simulations to estimate the binding free energy by the FEP method.

### Free energy perturbation method

The docking method provides reasonable information about the location of binding pocket, but it is not accurate enough for estimating the binding energy due to omission of receptor dynamics and a limited number of trail positions of ligand. Therefore, we further refined the docking results by a more expensive but accurate FEP method (23).

In the FEP method, the free energy difference between two states *A* and *B* is obtained using MD simulation during which the Hamiltonian of the system changes from *A* Hamiltonian to the *B* Hamiltonian through so-called $\lambda$ intervals. The transformation must be performed when a system remains in equilibrium state. The coupling parameter $\lambda$ is

used to modify the Hamiltonian from pure state $A$ ($\lambda = 0$) to pure state $B$ ($\lambda = 1$). The change of free energy between two state $\lambda_i$ and $\lambda_{i+1}$, $\triangle G_{\lambda i \rightarrow} \lambda_{i+1}$, can be determined by Bennett's acceptance ratio (BAR) (59). Then, the free energy difference between state $A$ and state $B$ is sum over the intervals:

$$\Delta G = \sum_{\lambda_0}^{\lambda_1} \Delta G_{\lambda_i \rightarrow \lambda_{i+1}} \tag{1}$$

Here,

$$\Delta G_{\lambda_i \rightarrow \lambda_{i+1}} = \int_{\lambda_i}^{\lambda_{i+1}} \left\langle \frac{\partial H(\lambda)}{\partial \lambda} \right\rangle_{\lambda'} d\lambda' \tag{2}$$

$H$ is Hamiltonian of the system.
The Coulomb interaction between two atoms depends on $\lambda$ as follows

$$V_C = \frac{f}{\varepsilon_{rf} r_{ij}} \left[ (1-\lambda) q_i^A q_j^A + \lambda q_i^B q_j^B \right] \tag{3}$$

where $f = 1/4\pi\varepsilon_0$.
For the vdW interaction, one has

$$V_{vdw} = \frac{(1-\lambda)C_{12}^A + \lambda C_{12}^B}{r_{ij}^{12}} - \frac{(1-\lambda)C_6^A + \lambda C_6^B}{r_{ij}^6} \tag{4}$$

The similar expressions for local interaction energies may be found in the GROMACS manual (47).

In a free energy calculation where particles appear or disappear, the use of the simple linear interpolation of the Lennard-Jones and Coulomb potentials as described in eqn 3 and eqn 4 may lead to poor convergence. When the particles have nearly disappeared, or are close to appearing (at $\lambda$ close to 0 or 1), the interaction energy will be weak enough for particles to get very close to each other, leading to large fluctuations in values of $\partial V/\partial\lambda$.

To overcome these difficulties, the singularities in the potentials need to be removed by modifying the regular Lennard-Jones and Coulomb potentials with 'soft-core' potentials that limit the energies and forces involved at values between 0 and 1, but not at $\lambda = 0$ or 1. In GROMACS, the soft-core potentials $V_{SC}$ are modified versions of the regular potentials, so that the singularity in the potential and its derivatives at $r = 0$ is never reached:

$$V_{SC} = (1-\lambda)V^A(r_A) + \lambda V^B(r_B) \tag{5}$$

$$r_A = (\alpha\sigma_A^6\lambda^p + r^6)^{1/6} \tag{6}$$

$$r_B = (\alpha\sigma_B^6\lambda^p + r^6)^{1/6} \tag{7}$$

where $V^A$ and $V^B$ are the normal van der Waals or electrostatic potentials in state $A$ ($\lambda = 0$) and state $B$ ($\lambda = 1$), respectively, $\alpha$ is the soft-core parameter, $p$ is the soft-core $\lambda$ power, and $\sigma$ is the radius of the interaction. In our simulations, $p = 2$ and $\alpha = 1.5$ (60). Then, the derivative

$$\frac{\partial V_{SC}(r)}{\partial\lambda} = V^B(r_B) - V^A(r_A) + \frac{p\alpha}{6}\left[\lambda F^B(r_B) r_B^{-5}\sigma_B^6(1-\lambda)^{p-1} - (1-\lambda)F^A(r_A)r_A^{-5}\sigma_A^6\lambda_A^{p-1}\right] \tag{8}$$

can be used for estimation of the free energy with the help of eqn 2.
In the double-annihilation binding free energy method (61–63), the binding free energy of ligand to protein $\triangle G_{\text{bind}}$ is determined as the difference between $\triangle G_2$ and $\triangle G_1$ ($\triangle G_2 - \triangle G_1$), where $\triangle G_1$ is the free energy change associated with removal of a ligand to the gas phase from protein complexed with the ligand in solution and $\triangle G_2$ is the free energy change of removal of a ligand from the bulk solvent to the gas phase. Thus, the double-annihilation binding free energy method requires the calculation of free energy not only for the solvated complex but also for solvated ligand.

In this study, the non-bonded interactions between the ligands and other molecules were parameterized by the coupling parameter $\lambda$. We used 21 $\lambda$ points to reduce the vdW interaction and 12 $\lambda$ points to reduce the Coulomb interaction with a soft-core potential (62,63). For both the solvated complex and ligand systems, $\lambda$ = 0.0, 0.1, 0.2, 0.275, 0.375, 0.45, 0.55, 0.65, 0.675, 0.725, 0.75, 0.775, 0.8, 0.825, 0.85, 0.875, 0.9, 0.925, 0.95, 0.975, and 1.0 for the vdW interaction and $\lambda$ = 0.00, 0.10, 0.25, 0.45, 0.55, 0.65, 0.70, 0.75, 0.80, 0.90, 0.95, and 1.00 for the electrostatic interaction. Thus, one has to perform a total 33 independent MD simulations with different $\lambda$ but keeping the same randomly generated initial momentum distributions and configurations. Each MD simulation with a given value of $\lambda$ lasts for 1 ns. Then, the free energies were calculated by BAR (59) between $\lambda$ states (61–63) through potential energy differences between independent samples neighboring in $\lambda$. The results were collected from 4 independent trajectories for the complexes with AC1NX476, darunavir 1, and darunavir 2 and 1 trajectory for the complex WT+ritonavir.

### Tools and measures used for data analysis

A hydrogen bond (HB) was formed if the distance between donor D and acceptor A is ≤3.5 Å and the D-H-A angle is ≥135 degrees. A non-bonded contact (NBC), that is, contact between atoms that are neither covalently bonded, nor interacting via hydrogen bonds, is defined as contact between atom C or S of ligand and any atom of either protein or water molecules when the distance between them falls in the range of 2.9–3.9 Å. The HBs and NBCs were analyzed using LigPlot++ version 1.44 (64).

The electrostatic and vdW interaction energies were calculated to uncover factors that may play an important role in the ligand binding process.

## Results and Discussion

### *Docking results and initial structures for MD simulations*

We first checked the docking protocol for WT+ritonavir and WT+darunavir for which PDB structures are available. As the best docking pose of these ligands in the binding pocket is almost the same as in PDB structures, the Autodock Vina used in this work is reliable.

Because holo-structures of WT+AC1NX476, MT1+AC1NX 476, MT2+AC1NX476, and MT3+AC1NX476 are still unavailable in PDB, the Autodock Vina 1.1 has been employed to predict the pose of AC1NX476 in the binding site. The PDB apo structures, obtained from PDB holo-structures by removing ligand, were used for docking (Table S1). To achieve high accuracy, the exhaustiveness parameter in Autodock Vina (65) was set equal 4000 for AC1NX476 (66,67).

The hydrogen bonds and NBCs between AC1NX476 and WT in the best (lowest binding energy) docking mode (Figure S4) were studied by the HBPLUS program (68) and visualized by LigPlot++ version 1.44 (64). One can show that AC1NX476 has three hydrogen bonds with Asp29-A, Asp30-A, and Asp30-B. Ten residues from chain A, Asp25-A, Gly27-A, Asp29-A, Asp30A, Val32-A, Ile47-A, Gly48-A, Gly49-A, Ile50-A, and Ile84-A, and 11 residues from chain B, Asp25-B, Asp27-B, Ala28-B, Asp30-B, Val32-B, Gly48-B, Gly49-B, Ile50-B, Pro81-B, Val82-B, and Ile84-B, experience the interaction with ligand (Figure S4).

Only one HB between AC1NX476 and residue Gly27-B of MT1 has been found, but there are 25 NBCs with residues Arg8-A, Asp25-A, Asp29-A, Asp30-A, Val32-A, Ile47-A, Gly48-A, Gly49-A, **Val50-A**, Pro81-A, Val82-A, Ile84-A, Asp25-B, Gly27-B, Ala28-B, Asp29-B, Asp30-B, Val32-B, Ile47-B, Gly48-B Gly49-B, **Val50-B**, Phe52-B, Phe53-B, and Ile84-B (Figure S5). Note that two mutation points **Val50-A** and **Val50-B** belong to this list.

The list of MT2 residues, which have non-bonded interactions with AC1NX476 (Figure S6), contains Asp25-A, Gly27-A, Ala28-A, Asp29-A, Asp30-A, Val32-A, Ile47-A, Gly48-A, Gly49-A, Ile50-A, **Phe82-A**, **Val84-A**, Asp25-B, Gly27-B, Ala28-B, Asp29-B, Asp30-B, Val32-B, Ile46-B Ile47-B, Gly48-B, Gly49-B, Ile50-B, **Phe82-B**, and **Val84-B**. Among them, Asp29-B and Gly48-B also form HB with the ligand, while **Phe82-A**, **Val84-A**, **Phe82-B**, and **Val84-B** are mutation points.

In the best docking mode of complex MT3+AC1NX476, although MT3 has 28 point mutations, only four residues **Val50-A**, **Val50-B**, **Ala82-A**, and **Ala82-B** participate in the NBC network with other 20 residues (Leu23-A, Asp25-A, Gly27-A, Ala28-A, Asp29-A, Asp30-A, Val32-A, Gly48-A, Ile84-A, Leu23-B, Asp25-B, Asp27-B, Ala28-B, Asp30-B, Val32B, Gly48-B, Gly49-B, Pro81-B, and Ile84-B) (Figure S7). The residues Asp29-A, Asp30-A, and Asp30-B also form HB with AC1NX476.

Using the structures obtained in the best docking mode (Figure S3) and the software DoGSiteScorer (69), one can show that in the presence of AC1NX476, the volume of binding cavity is $\approx$ 897, 873, 1038, and 775 $\AA^3$ for WT, MT1, MT2, and MT3, respectively. Thus, the mutations alter not only the network of HBs and hydrophobic interactions but also the geometry of the active site of receptor. In addition, among mutation points, only residues **Val50-A** (MT1 and MT3), **Thr80-A** (MT2), **Ala82-A** (MT3), **Val84-A** (MT2), **Val50-B** (MT1 and MT3), and **Ala82-B** (MT2 and MT3) directly impact on the AC1NX476 binding affinity.

The X-ray diffraction structure of the complex WT+ritonavir, taken from PDB, was used to analyze non-bonded interactions. The NBC network includes 21 residues (Asp25-A, Gly27-A, Ala28-A, Asp29-A, Gly48-A, Gly49-A, Ile50-A, Val82-A, Ile84-A, Arg8-B, Asp25-B, Gly27-B, Ala28-B, Asp29-B, Asp30-B, Val32-B, Gly48-B, Gly49-B, Ile50-B, Pro81-B, and Val82-B) (Figure S8). Ritonavir also binds to Gly27-A, Asp29-A, Gly48-A, and Asp30-B via hydrogen bonding. Therefore, ritonavir, which has the binding energy to the HIV-1 PR WT higher than AC1NX476, has more HBs, but the number of NBCs is less suggesting that the hydrophobic interaction dominates over the hydrogen bonding.

Darunavir has two possible positions in the experimentally resolved structure with WT (PDB ID: 4LL3). In position 1, darunavir has five HBs with Asp25-A, Asp30-A, Glu27-B, and Asp29-B (Figure S9), while it forms only 3 HBs with residues Gly27-A, Asp29-A, and Asp25-B in position 2 (Figure S10). WT interacts with darunavir in position 1 through 18 residues, Asp25-A, Gly27-A, Ala28-A, Asp30-A, Val32-A, Gly48-A, Gly49-A, Pro81-A, Ile84-A, Leu23-B, Asp25-B, Gly27-B, Ala28B, Asp29-B, Val32-B, Gly48-B, Gly49-B, and Ile150-B by NBC. In position 2, NBC network involves 19 residues, Leu23-A, Asp25-A, Gly27-A, Ala28-A, Asp30-A, Gly48-A, Gly49-A, Ile50-A, Arg8-B, Asp25-B, Gly27-B, Ala28-B, Asp30-B, Val32-B, Gly48-B, Gly49-B, Pro81-B, Val82-B, and Ile84-B (Figures S9 and S10). Thus, our analysis revealed that both HB and NBC networks contribute to the ligand-binding affinity for all systems studied.

### *Results obtained by molecular dynamics simulations*

#### Equilibration step

We have performed 4 independent 20 ns NPT runs for each complex of AC1NX476 bound to HIV-1 PR sequences, WT+darunavir1 and WT+darunavir 2. The conformations obtained in the best docking mode were used as starting

configurations for complexes with AC1NX476, while for WT+darunavir 1 and WT+darunavir 2, the MD runs started from the PDB holo-structure 4LL3 (Figure S3). For the WT+ritonavir, one MD trajectory was performed starting from the PDB structure 2HXW. As evident from Figure 2, all systems reached the equilibrium after about 5 ns except trajectory 3 of WT+AC1NX476 and trajectory 4 of MT1+AC1NX476, where the equilibration time is about 15 ns. The fluctuations of $C\alpha$ atoms relative to their initial positions in WT and mutations in the presence of AC1NX476 are typically larger than those of WT bound with ritonavir and darunavir (Figure 3). The magnitude of thermal fluctuations of complexes is quite small with $C\alpha$ RMSD remaining below 2.5 Å as the systems are stable in equilibrium.

## Ligand–receptor interaction

We consider the last snapshots, obtained in the previous 20 ns NPT runs, in detail because they will be used as starting configurations for the final 1 ns MD simulations for estimating the binding free energy by the BAR method. Figures S11–S16 in SI show such snapshots for the WT+AC1NX476, MT1+AC1NX476, MT2+AC1NX476, MT3+AC1NX476, WT+ritonavir, WT+darunavir 1, and WT+darunavir 2, respectively. Their NBC and HB networks are analyzed, and the results are shown in Table 1. The mean number of HBs between AC1NX476 and receptors varies between 2 and 3.25, while for WT+ritonavir and WT+darunavir, one has 4 and 3.75 contacts, respectively. The result for WT+darunavir was obtained as an average over 8 snapshots of WT+darunavir 1 and WT+darunavir 2.

The number of NBCs is much higher than HBs falling in the range of 16–22. As follows from the per-residue distributions of interaction energies between ligands and HIV-1 PR variants (Figure 4), for WT, residues Asp25-A, Gly48-A, and Asp25-B dominate having not only long-live HBs but also NBCs with the ligand. In the case of MT1+AC1NX476, the ligand interacts with 33 residues

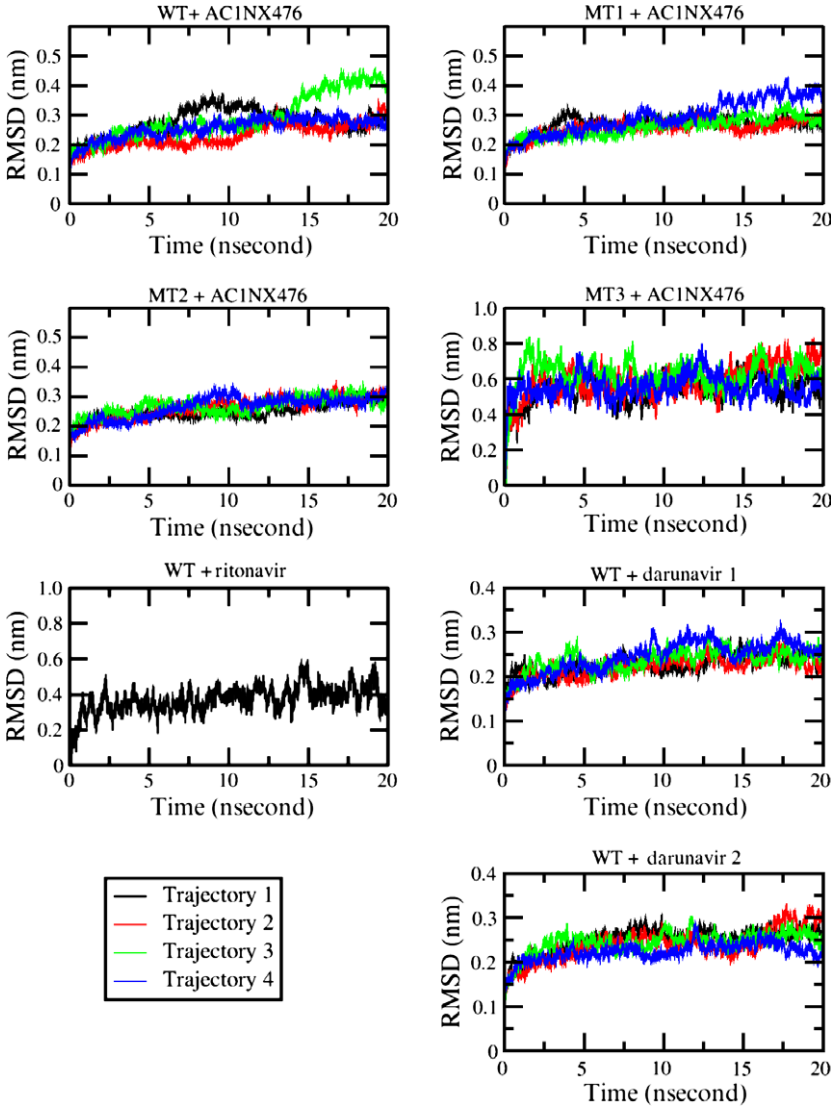


**Figure 2:** Time dependence of RMSD for five solvated complexes: AC1NX476 bound to WT, MT1, MT2, and MT3, ritonavir bound to WT, and darunavir position 1 and position 2 bound to WT.

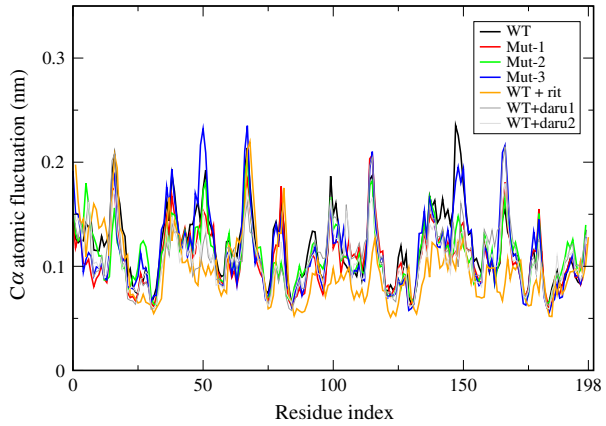


**Figure 3:** Cα atomic fluctuation of HIV-1 protease WT and their mutations in the solvated complexes with AC1NX476, ritonavir, and darunavir (daru1 is darunavir in position 1 and daru2 is darunavir in position 2). Results were averaged over 20 ns of MD simulations.

**Table 1:** The mean number of HBs and contacts between ligands and the receptors and between ligands and water molecules in the binding pocket

| Complexes | Volume of binding cavity (Å$^3$) | $N_{WM}^{NBC}$ | $N_{WM}^{HB}$ | $N_{res}^{NBC}$ | $N_{res}^{HB}$ |
|---|---|---|---|---|---|
| WT+AC1NX476 | 922.39 | 17 | 6.75 | 19.75 | 2 |
| MT1+AC1NX476 | 1002.65 | 24.25 | 6.75 | 17.5 | 3.25 |
| MT2+AC1NX476 | 980.84 | 16 | 6.5 | 16.25 | 2 |
| MT3+AC1NX476 | 989.92 | 21.25 | 7.25 | 18.5 | 2.75 |
| WT+Ritonavir | 928.77 | 23 | 8 | 20 | 4 |
| WT+Darunavir | 901.94 | 6.25 | 7 | 21.63 | 3.75 |

Results are averaged over 4 snapshots for complexes of AC1NX476 bound with HIV-1 protease structures and darunavir bound to two positions of WT. In the case of WT+ritonavir, the result was obtained using one snapshot. $N_{WM}^{HB}$ and $N_{WM}^{NBC}$ stand for the number of water molecules that have the HB and NBC with ligand. $N_{res}^{HB}$ and $N_{res}^{NBC}$ refer to the number of residues interacting with ligand via HB and NBC. Non-integer numbers of residues and water molecules come from averaging over several snapshots.

among which Asp25-A, Asp29-A, Ile47-A, Gly48-A, Gly49-A, Thr80-A, and Val82-A are the most active (Figure 4). The mutation point **Val50-A** also substantially affects the binding affinity. **Phe82-A**, **Val84-A**, **Phe82-B**, and **Val84-B** are the mutation points of MT2 which have the strong interaction with AC1NX476. There exist only 30 residues of MT2 that had the non-bonding interaction with AC1NX476 against 34 residues of MT3 (Figure 4). The residues Arg8-A, Asp30-A, Asp25-B, Asp129, Ile47-B, Gly48-B, Ile50-B, and **Phe82-B** are the most prominent for MT2, while for MT3, such residues are Asp29-A, Asp30-A, Ile47-A, Gly48-A, Gly49-A, Gly51-A, and Arg87-A (Figure 4). The mutation points **Ile46-A** and **Val50-A** greatly impact on the binding of AC1NX476 to MT3.

The per-atom interaction energy (vdW and electrostatic) for AC1NX476 in complex with HIV-1 PR sequences was calculated in water (Figure S17). Overall, atoms O9, C42, O10, C29, S1, O7, O8, N13, N14, C47, and C48 are the most relevant in the binding mode of all variants. The presence of electronegative atoms O9, O10, C29, O7, O8, N13, N14, and C48 enhances the binding affinity, while electropositive atoms C42, S1, and C47 reduce it. In the WT+AC1NX476 case, although the mean electrostatic interaction energy (-35.14 kcal/mol) is 33.1% of the total interaction energy (-106.15 kcal/mol) for solvated complex systems, we observed the strong correlation not only between atom charges of AC1NX476 and the electrostatic interaction energy ($R$ = 0.892), but also between atomic charges of AC1NX476 and the total interaction energy ($R$ = 0.893) (Figure 5). Figure 5 plots the mean values of interaction energies for four complexes as a function of atomic charges, but the overall correlation also holds for individual systems (results not shown). The increase of $\triangle G_{bind}$ with increasing atomic charges is in line with the fact that C42, C47, and S1 reduce the binding affinity and a ligand with more electronegative atoms should be more prone in binding to HIV-1 PR.

One can show that the vdW interaction between AC1NX476 and HIV-1 PR sequences dominates over the electrostatic interaction. This remains valid even when a more precise free energy perturbation method is applied (see Table 2 below).

## Ligand–water interaction

Because water molecules in the binding pocket play the important role (14,15,70,71), we study their interaction with ligands in detail. The ligands form more HBs with water molecules than with the protein (Table 1), and the number of HBs is not very sensitive to sequences and ligands varying between 5 and 8. In equilibrium, AC1NX476 has NBC with 17 water molecules inside the binding pocket of WT (Table 1). In the case of MT1, this number levels up to 24.75 with 6.25 water molecules having hydrogen bonding with AC1NX476. In complexes MT2+AC1NX476 and MT3+AC1NX476, there were 16 and 21.25 water molecules that have NBC with the ligand, respectively (Table 1). The ritonavir has contact with 23 water molecules including 8 HBs. The darunavir in position 1 and position 2 has 7 HBs and 6.25 NBCs with water molecules, respectively. As shown below, the binding affinity is correlated with the number of water molecules inside the binding pocket that interact with ligand.

### *Estimation of binding free energy by BAR method*

Using the last snapshots obtained in the previous 20 ns NPT runs (Figures S11–S16), we have performed 1 ns MD runs with different values of $\lambda$. The binding free energy has been estimated using the double-annihilation binding free energy method, where the free energy was computed

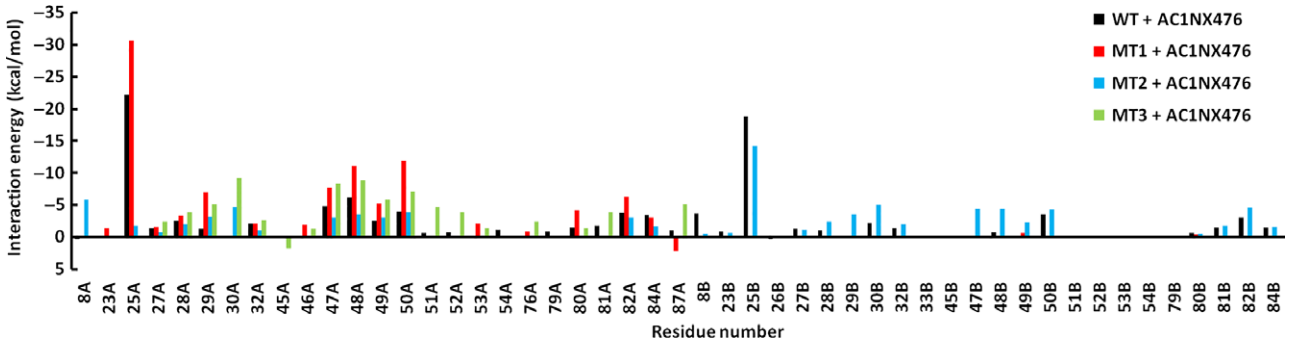


**Figure 4:** Per-residue interaction energy of HIV-1 protease wild type and their mutations with AC1NX476. The mutation points are highlighted by star.

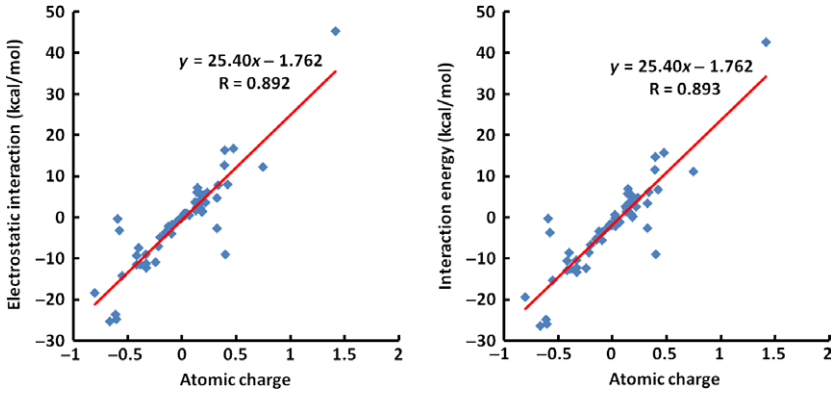


**Figure 5:** The correlation between atomic charges of AC1NX476 and the total interaction energy (right) and electrostatic interaction energy (left) per atom. The results were averaged over four sequences WT, MT1, MT2, and MT3.

**Table 2:** The binding energy estimated by the docking ($\triangle E_{bind}$ and FEP ($\triangle G_{FEP}$) methods

| | $\triangle E_{bind}$ | $\Delta G_{FEP}^{elec}$ | $\Delta G_{FEP}^{vdw}$ | $\triangle G_{FEP}$ | $\triangle G_{exp}$ |
|---|---|---|---|---|---|
| WT+AC1NX476 | −9.40 | −1.98 | −20.07 | −22.05 | −19.54 |
| MT1+AC1NX476 | −9.80 | −4.94 | −13.74 | −18.64 | −15.92 |
| MT2+AC1NX476 | −9.60 | −0.10 | −19.59 | −19.69 | −17.00 |
| MT3+AC1NX476 | −10.00 | 1.79 | −20.87 | −19.08 | −16.17 |
| WT+Ritonavir | −6.00 | −1.83 | −16.22 | −18.05 | −14.70 |
| WT+Darunavir | −7.00 | 3.63 | −22.29 | −18.66 | −15.90 |

The experimental binding free energy was calculated from formula $\triangle G_{exp} = RT\ \ln K_i$, where gas constant $R$ = 1.987 kcal/K/mol, $T$ = 300 $K$, and inhibition constant $K_i$ is measured in mol. Energy is measured in kcal/mol. The result for WT+darunavir was averaged over two positions.

from each circle of 50 ps. Initially, it fluctuates a bit (Figure 6) because the coupling parameter $\lambda$ varies among 33 different values. The free energy of solvated protein–ligand complex converges after 300 ps, while for the solvated ligand, it starts to saturate after about 100 ps. In the annihilation method, the binding free energy is estimated as the difference between the free energies of the solvated protein–ligand complex and solvated ligand (lower panel of Figure 6). Finally, averaging over the equilibrium time window ($t$ > 300 ps), we obtain the binding free energies for six systems (Table 2).

## High correlation between experimentally measured and calculated binding free energies

Figure 7 shows the experimental binding free energies ($\triangle G_{exp}$) versus calculated binding free energies ($\triangle G_{FEP}$) for six complexes. $G_{exp}$ were estimated by formula $\triangle G_{exp} = RT\ \ln K_i$ where the gas constant $R$ = 1.987 kcal/K/mol, $T$ = 300 k, and inhibition constant $K_i$ is measured in mol. The theoretical results are in excellent agreement with the experimental data with the correlation level $R$ = 0.993. However, the linear fit line in Figure 7 gives $\triangle G_{exp} = 1.146 \times \triangle G_{FEP} + 5.652$ implying that although the correlation is nearly perfect, computed free energies are more negative than the experimental values by about 3 kcal/mol. Using the GROMOS96 43a1 force field and SPC water model, in accord with our finding, one obtained the free energy of solvated side-chain analogs in water of the amino acids smaller than the experimental data (72,73). Thus, the GROMOS96 43a1 force field with SPC water model and BAR method can be used to explain the ranking of binding affinities of AC1NX476 to HIV-1 PR sequences WT > MT2 > MT3 > MT1.

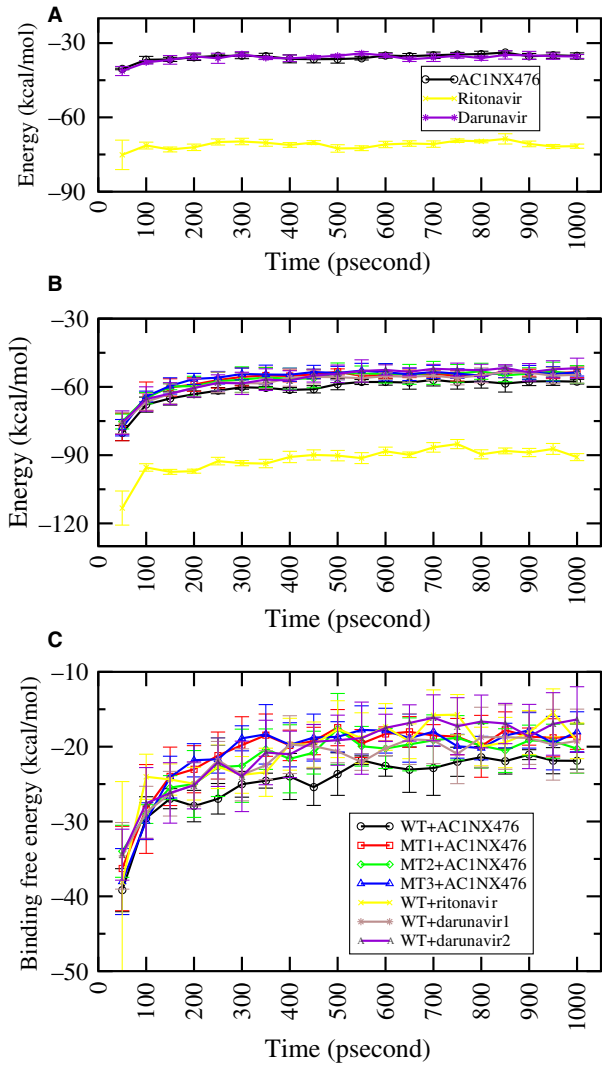


**Figure 6:** (A) The free energy of solvated AC1NX476 and ritonavir alone. (B) The free energy of solvated complexes WT+AC1NX476, MT1+AC1NX476, MT2+AC1NX476, MT3+AC1NX476, WT+ritonavir, WT+darunavir position 1, and WT+darunavir position 2. (C) Time dependence of binding free energies for seven complexes. The values collected in the equilibrium region ($t$ > 300 ps) were used to calculate ΔGFEP. The error bars show the root mean square deviations.

As evident from Table 2, darunavir binds to WT stronger than ritonavir. However, the binding affinity of darunavir to WT is lower than AC1NX476 to the same target. The binding free energy of AC1NX476 to MT1 and MT3 is almost the same as darunavir to WT.

## vdW interaction plays a key role in ligand binding to HIV-1 PR sequences

The contributions of vdW and Coulomb interactions to the binding free energy are shown in Table 2. Clearly, in all cases, the electrostatic interaction contributes to $\triangle G_{bind}$ to less extent than the former implying that the vdW interaction is a driving force for ligand binding.

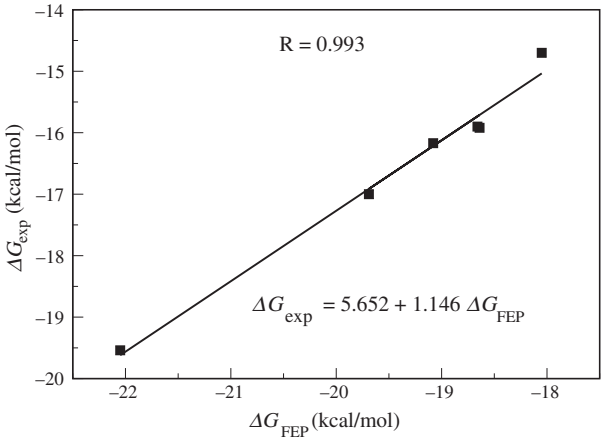


**Figure 7:** The correlation between experimentally measured and theoretical estimations of binding free energies for five complexes.

## Binding affinity deteriorates with increase of the number of water molecules interacting with ligand

As evident from Figure S18, there is no correlation between $\triangle G_{bind}$ and the number of water molecules that form HBs with ligand inside the binding pocket ($R$ = 0.24). However, the binding free energy is correlated with the number of water molecules in equilibrium (Table 1 and Figure S18) which have non-bonding interaction with inhibitors ($R$ = 0.691). This is in good agreement with the experiments (70) and previous theoretical works (15,71) that the binding gets weaker as the number of water molecules in the binding pocket increases because the water screens the interaction between the ligand and receptor. Due to domination of the vdW interaction, $\triangle G_{bind}$ decreases with the number of receptor residues interacting with AC1NX476 via NBC. Although the binding affinity is correlated with the number of residues that form HB with the ligand ($R$ = 0.76), it is hard to make any certain conclusion as $N_{res}^{HB}$ varies in a rather narrow window (Figure S18).

## Binding free energy correlates with volume of binding cavity

The mutations alter the volume of protein binding cavity (Table 1). WT with AC1NX476, ritonavir, and darunavir has relatively small binding site, while the mutations widen it. This leads to lower binding affinities as shown in the experiments and our simulations. For AC1NX476, the binding affinities to 4 sequences correlate with the volume of binding pocket almost perfectly with the correlation level $R$ = 1 (Figure S18).

## Conclusions

We have studied the effect of mutations on the binding of AC1NX476 to HIV-1 PR sequences. The correlation between theoretically computed and experimentally measured $\triangle G_{bind}$ is excellent although their absolute values are different by about 3 kcal/mol. This agreement implies that the parameterization of ligands, where atom type and bonding are generated by the PRODRG2 beta server and the charge groups obtained by RESP method at the Hartree–Fock (HF)/6-31G(d) level in the gas phase, is suitable. In addition, the Gromos96 43a1 force field in combination with the SPC water model is a reasonable choice.

It has been shown that the vdW interaction is more important than the electrostatic interaction in binding of AC1NX476, ritonavir, and darunavir to HIV-1 PR sequences. Residues Asp25-A, Asp29-A, Asp30-A, Ile47-A, Gly48-A, and Asp25-B and the mutation points **Ile46-A** (MT3), **Val50-A** (MT1 and MT3), **Phe82-A**, **Val84-A**, **Phe82-B**, and **Val84-B** (MT2) strongly impact on the binding affinity. The electronegative atoms of ligand were found to enhance the binding affinity to a greater extent than the electropositive ones.

Our study revealed the binding mechanism of ligands to HIV-1 PR variants in such a way that mutations alter the binding affinity by modulating the volume of the binding pocket and the number of water molecules inside it. The smaller is the number of water molecules that have the interaction with ligand, the stronger is their binding. The binding affinity of AC1NX476 to HIV-1 PR sequences levels up with decrease of the binding cavity volume. It would be interesting to perform *in vivo* studies on the possibility of using AC1NX476 as a potential medicine for HIV as its binding affinity to HIV-1 PR sequences is better than darunavir.

## Future Directions

Our future work will be focused on the impact of various mutations on the binding affinity of AC1NX476. Another direction of research is to screen out potential HIV-1 PR inhibitors, which are more efficient than available drugs, from databases by computer simulation combined with *in vitro* experiments.

## Acknowledgments

The work was supported by Narodowe Centrum Nauki in Poland (Grant No 2011/01/B/NZ1/01622) and Department of Science and Technology at Ho Chi Minh city, Vietnam. Allocation of CPU time at the supercomputer center TASK in Gdansk (Poland) is highly appreciated.

## References

1. UNAIDS. Global report: Report on the Global AIDS Epidemic. www.unaids.org: 2012.
2. UNAIDS. World AIDS Day Report: Results. www.unaids.org: 2012.
3. UNAIDS. AIDS at 30: Nations at the crossroads. www.unaids.org: 2011.
4. Clercq D.E. (2007) The design of drugs for HIV and HCV. Nat Rev Dru Dis;6:1001–1018.
5. Clercq D.E. (2009) Anti-HIV drugs: 25 compounds approved within 25 years after the discovery of HIV. Int J Antimicrob Ag;33:307–320.
6. de Bethune M.P. (2010) Non-nucleoside reverse transcriptase inhibitors (NNRTIs), their discovery, development, and use in the treatment of HIV-1 infection: a review of the last 20 years (1989–2009). Antiviral Res;85:75–90.
7. Surleraux D.L., Tahri A., Verschueren W.G., Pille G.M., de Kock H.A., Jonckers T.H., Peeters A., De Meyer S., Azijn H., Pauwels R., de Bethune M.P., King N.M., Prabu-Jeyabalan M., Schiffer C.A., Wigerinck P.B.T.P, (2005) Discovery and selection of TMC114, a next generation HIV-1 protease inhibitor. J Med Chem;48:1813–1822.
8. Clavel F., Hance A.J. (2004) HIV drug resistance. N Eng J Med;350:1023–1035.
9. Richman D.D. (2001) HIV chemotherapy. Nature;410:995–1001.
10. Zoete V., Michielin O., Karplus M. (2003) Protein-ligand binding free energy estimation using molecular mechanics and continuum electrostatics. Application to HIV-1 protease inhibitors. J Comput Aid Mol Des;17:861–880.
11. Oehme D.P., Brownlee R.T., Wilson D.J. (2012) Effect of atomic charge, solvation, entropy, and ligand protonation state on MM-PB(GB)SA binding energies of HIV protease. J Comput Chem;33:2566–2580.
12. Wright D.W., Hall B.A., Kenway O.A., Jha S., Coveney P.V. (2014) Computing clinically relevant binding free energies of HIV-1 protease inhibitors. J Chem Theory Comput;10:1228–1241.
13. Berti F., Frecer V., Miertus S. (2014) Inhibitors of HIV-protease from computational design. A history of theory and synthesis still to be fully appreciated. Curr Pharm Design;20:3398–3411.
14. Hamelberg D., McCammon J.A. (2004) Standard free energy of releasing a localized water molecule from the binding pockets of proteins: double-decoupling method. J Am Chem Soc;126:7683–7689.
15. Lu Y., Yang C.Y., Wang S. (2006) Binding free energy contributions of interfacial waters in HIV-1 protease/inhibitor complexes. J Am Chem Soc;126:11830–11839.
16. Aruksakunwong O., Wolschann P., Hannongbua S., Sompornpisut P. (2006) Molecular dynamic and free

energy studies of primary resistance mutations in HIV-1 protease-ritonavir complexes. J Chem Inf Model;46: 2085–2092.
17. Meher B.R., Wang Y.X. (2012) Interaction of I50V mutant and I50L/A71V double mutant HIV-protease with inhibitor TMC114 (darunavir): molecular dynamics simulation and binding free energy studies. J Phys Chem B;116:1884–1900.
18. Srinivasan J., Cheatham T.E., Cieplak P., Kollman P.A., Case D.A. (1998) Continuum solvent studies of the stability of DNA, RNA, and phosphoramidate–DNA helices. J Am Chem Soc;120:9401–9409.
19. Leonis G., Czyznikowska Z., Megariotis G., Reis H., Papadopoulos M.G. (2012) Computational studies of darunavir into HIV-1 protease and DMPC bilayer: necessary conditions for effective binding and the role of the flaps. J Chem Inf Model;52:1542–1558.
20. Tzoupis H., Leonis G., Mavromoustakos T., Papadopoulos M.G. (2013) A comparative molecular dynamics, MM-PBSA and thermodynamic integration study of saquinavir complexes with wild-type HIV-1 PR and L10I, G48V, L63P, A71V, G73S, V82A and I84V single mutants. J Chem Inf Model;9:1754–1764.
21. Hanlon M.H., Porter D.J.T., Furfine E.S., Spaltenstein A., Carter H.L., Danger D. *et al.* (2004) Inhibition of wild-type and mutant human immunodeficiency virus type 1 protease by gw0385 and other arylsulfonamides. Biochem;43:14500–14507.
22. Spaltenstein A., Almond M.R., Bock W.J., Cleary D.G., Hazen R.J., Kazmierski W.M. *et al.* (2000) Novel inhibitors of HIV protease: design, synthesis and biological evaluation of picomolar inhibitors containing cyclic P1/P2 scaffolds. Bioorg Med Chem Lett;10: 1159–1162.
23. Zwanzig R.W. (1954) High-temperature equation of state by a perturbation method. I. Nonpolar Gases. J Chem Phys;22:1420–1426.
24. Allouche A.-R. (2011) Gabedit-A graphical user interface for computational chemistry softwares. J Comput Chem;32:174–182.
25. Kempf D.J., Marsh K.C., Denissen J.F., MacDonald E., Vasavanonda S., Flentge C.A. *et al.* (1995) ABT-538 is a potent inhibitor of human immunodeficiency virus protease and has high oral bioavailability in humans. Proc Natl Acad Sci USA;92:2484–2488.
26. Kozisek M., Lepsik M., Saskova K.G., Brynda J., Konvalinka J., Rezacova P. (2014) Thermodynamic and structural analysis of HIV protease resistance to darunavir – analysis of heavily mutated patient-derived HIV-1 proteases. FEBS J;281:1834–1847.
27. Bottcher J., Blum A., Heine A., Diederich W.E., Klebe G. (2008) Structural and kinetic analysis of pyrrolidine-based inhibitors of the drug-resistant Ile84Val mutant of HIV-1 protease. J Mol Biol;383:347–357.
28. Schrödinger LLC A. The AxPyMOL Molecular Graphics Plugin for Microsoft PowerPoint, Version 1.1 2010.
29. Schrödinger LLC J. The JyMOL Molecular Graphics Development Component, Version 1.0 2010.
30. Schrödinger LLC P. The PyMOL Molecular Graphics System, Version 1.3r1 2010.
31. Miller J.F., Andrews C.W., Brieger M., Furfine E.S., Hale M.R., Hazen R.J. *et al.* (2006) Ultra-potent P1 modified arylsulfonamide HIV protease inhibitors: the discovery of GW0385. Bioorg Med Chem Lett;16:1788–1794.
32. Chen X.N., Tropsha A. (1995) Relative binding free energies of peptide inhibitors of HIV-1 protease- The influence of the active-site protonation state. J Med Chem;38:42–48.
33. Hyland L.J., Tomaszek T.A., Meek T.D. (1991) Human immunodeficiency virus-1 protease. 2. Use of pH rate studies and solvent kinetic isotope effects to elucidate details of chemical mechanism. Biochem;30:8454–8463.
34. Pietrucci F., Marinelli F., Carloni P., Laio A. (2009) Substrate binding mechanism of HIV-1 protease from explicit-solvent atomistic simulations. J Am Chem Soc;131:11811–11818.
35. Hou T., McLaughlin W.A., Wang W. (2008) Evaluating the potency of HIV-1 protease drugs to combat resistance. Proteins;71:1163–1174.
36. Li H., Robertson A.D., Jensen J.H. (2005) Very fast empirical prediction and rationalization of protein pKa values. Proteins;61:704–721.
37. Bas D.C., Rogers D.M., Jensen J.H. (2008) Very fast prediction and rationalization of pKa values for protein-ligand complexes. Proteins;73:765–783.
38. Olsson M.H.M., Søndergaard C.R., Rostkowski M., Jensen J.H. (2011) PROPKA3: consistent treatment of internal and surface residues in empirical pKa predictions. J Chem Theo Comp;7:525–537.
39. Sondergard C.R., Olsson M.H.M., Rostkowski M., Jensen J.H. (2011) Improved treatment of ligands and coupling effects in empirical calculation and rationalization of pKa values. J Chem Theo Comp;7:2284–2295.
40. Sanner M.F. (1999) Python: a programming language for software integration and development. J Mol Graphics Mod;17:57–61.
41. Trott O., Olson A.J. (2010) Improving the speed and accuracy of docking with a new scoring function, efficient optimization, and multithreading. J Comput Chem;31:455–461.
42. Bohm H.J. (1994) The development of a simple empirical scoring function to estimate the binding constant for a protein-ligand complex of known three-dimensional structure. J Comput Aid Mol Des;8:243–256.
43. Mihajlovic M.L., Mitrasinovic P.M. (2009) Applications of the ArgusLab4/AScore protocol in the structure-based binding affinity prediction of various inhibitors of group-1 and group-2 influenza virus neuraminidases (NAs). Mol Sim;35:311–324.
44. Shanno D.F. (1970) Conditioning of Quasi-Newton methods for function minimization. Math Comp;24:647–656.
45. Morris G.M., Godsell D.S., Halliday R.S., Huey R., Hart W.E., Belew R.K. *et al.* (1998) Automated docking using

a lamarckian genetic algorithm and an empirical binding free energy function. J Comput Chem;19:1639–1662.
46. Morris G.M., Goodsell D.S., Huey R., Olson A.J. (1996) Distributed automated docking of flexible ligands to proteins: parallel applications of AutoDock 2.4. J Comput Aid Mol Des;10:293–304.
47. Hess B., Kutzner C., van der Spoel D., Lindahl E. (2008) Gromacs 4: algorithms for highly efficient, load-balanced, and scalable molecular simulation. J Chem Theory Comput;4:435–447.
48. van Gunsteren W.F., Billeter S.R., Eising A.A., Hunenberger P.H., Kruger P., Mark A.E. *et al.* (1996) Biomolecular Simulation: The GROMOS96 Manual and User Guide. Zurich: Vdf Hochschulverlag AG an der ETH.
49. Scott W.R.P., Hünenberger P.H., Tironi I.G., Mark A.E., Billeter S.R., Fennen J. *et al.* (1999) The GROMOS biomolecular simulation program package. J Phys Chem A;103:3596–3607.
50. Berendsen H.J.C., Postma J.P.M., vanGunsteren W.F., Hermans A.J.. (1981) Intermolecular Forces. Dordrecht: Reidel.
51. Nguyen T.T., Viet M.H., Li M.S. (2014) Effects of water models on binding affinity: evidence from all-atom simulation of binding of tamiflu to A/H5N1 neuraminidase. ScientificWorldJournal;2014:paper 536084.
52. Schuttelkopf A.W., van Aalten D.M.F. (2004) PRODRG: a tool for high-throughput crystallography of protein-ligand complexes. Acta Crystallogr Sect D Biol;60:1355–1363.
53. Lemkul J.A., Allen W.J., Bevan D.R. (2010) Practical considerations for building GROMOS-compatible small-molecule topologies. J Chem Inf Model;50:2221–2235.
54. Bayly C.I., Cieplak P., Cornell W., Kollman P.A. (1993) A well-behaved electrostatic potential based method using charge restraints for deriving atomic charges: the RESP model. J Phys Chem;97:10269–10280.
55. Van Gunsteren W.F., Berendsen H.J.C. (1988) A leap-frog algorithm for stochastic dynamics. Mol Sim;1:173–185.
56. Parrinello M., Rahman A. (1981) Polymorphic transitions in single crystals: a new molecular dynamics method. J Appl Phys;52:7182–7190.
57. Hess B., Bekker H., Berendsen H.J.C., Fraaije J.G.E.M. (1997) LINCS: a linear constraint solver for molecular simulations. J Comp Chem;18:1463–1472.
58. Darden T., York D., Pedersen L. (1993) Particle mesh Ewald: an N·log(N) method for Ewald sums in large systems. J Chem Phys;98:10089–10092.
59. Bennett C.H. (1976) Efficient estimation of free energy differences from Monte Carlo data. J Comput Phys;22:245–268.
60. Beutler T.C., Mark A.E., van Schaik R.C., Gerber P.R., van Gunsteren W.F. (1994) Avoiding singularities and numerical instabilities in free energy calculations based on molecular simulations. Chem Phys Lett;222:529–539.
61. Jorgensen W.L., Buckner J.K., Boudon S., Tirado-Rives J. (1988) Efficient computation of absolute free energies of binding by computer simulations. Application to the methane dimer in water. J Chem Phys;89:3742.
62. Jayachandran G., Shirts M.R., Park S., Pande V.S. (2006) Parallelized-over-parts computation of absolute binding free energy with docking and molecular dynamics. J Chem Phys;125:084901.
63. Fujitani H., Tanida Y., Ito M., Jayachandran G., Snow C.D. (2005) Direct calculation of the binding free energies of FKBP ligands. J Chem Phys;123:084108.
64. Laskowski R.A., Swindells M.B. (2011) LigPlot+: multiple ligand-protein interaction diagrams for drug discovery. J Chem Inf Model;51:2778–2786.
65. Chang M.W., Ayeni C., Breuer S., Torbett B.E. (2010) Virtual screening for HIV protease inhibitors: a comparison of AutoDock 4 and vina. PLoS ONE;5:e11955.
66. Ngo S.T., Li M.S. (2012) Curcumin binds to Abeta1-40 peptides and fibrils stronger than ibuprofen and naproxen. J Phys Chem B;116:10165–10175.
67. Ngo S.T., Li M.S. (2013) Top-leads from natural products for treatment of Alzheimer's disease: docking and molecular dynamics study. Mol Sim;39:279–291.
68. McDonald I.K., Thornton J.M. (1994) Satisfying hydrogen bonding potential in proteins. J Mol Biol;238:777–793.
69. Volkamer A., Kuhn D., Rippmann F., Rarey M. (2012) Combining global and local measures for structure-based druggability predictions. J Chem Inf Model;52:360–372.
70. Ben-Naim A., Marcus Y. (1984) Solvation thermodynamics of nonionic solutes. J Chem Phys;81:2016.
71. Mai B.K., Viet M.H., Li M.S. (2010) Top-leads for swine influenza A/H1N1 virus revealed by steered molecular dynamics approach. J Chem Inf Model;50:2236–2247.
72. Villa A., Mark A.E. (2002) Calculation of the free energy of solvation for neutral analogs of amino acid side chains. J Comput Chem;23:548–553.
73. Maccallum J.L., Tieleman D.P. (2003) Calculation of the water-cyclohexane transfer free energies of neutral amino acid side-chain analogs using the OPLS all-atom force field. J Comput Chem;24:1930–1935.

## Supporting Information

Additional Supporting Information may be found in the online version of this article:

**Figure S1** The chemical structure of AC1NX476 with atomic names.

**Figure S2** The two-dimensional chemical structure of ritonavir (A) and darunavir (B).

**Figure S3** Structures obtained in the best docking mode for AC1NX476 bound to WT (A), MT1 (B), MT2 (C), and MT3 (D), and X-ray diffraction structure of ritonavir bound

to WT (E), darunavir position 1 (red color) and position 2 (blue color) bound to WT (F). These structures were used as starting configurations for MD simulations.

**Figure S4** Hydrogen bonds (red line) and non-bonded contacts (represented by an arc with spokes radiating towards the ligand atoms they contact) between AC1NX476 and WT.

**Figure S5** Hydrogen bonds (red line) and non-bonded contacts between AC1NX476 and MT1.

**Figure S6** Hydrogen bonds (red line) and non-bonded contacts between AC1NX476 and MT2.

**Figure S7** Hydrogen bonds (red line) and non-bonded contacts AC1NX476 and MT3.

**Figure S8** Hydrogen bonds (red line) and non-bonded contacts between ritonavir and WT.

**Figure S9** Hydrogen bonds (red line) and non-bonded contacts between darunavir position 1 and WT.

**Figure S10** Hydrogen bonds (red line) and non-bonded contacts between darunavir position 2 and WT.

**Figure S11** The last snapshots of the complex WT+AC1NX476 obtained in 20 ns MD trajectories.

**Figure S12** The same as in Figure S11 but for MT1+AC1NX476.

**Figure S13** The same as in Figure S11 but for MT2+AC1NX476.

**Figure S14** The same as in Figure S11 but for MT3+AC1NX476.

**Figure S15** The same as in Figure S11 but for WT+ritonavir.

**Figure S16** The same as in Figure S11 but for WT+darunavir position 1 and 2.

**Figure S17** Per-atom interaction energy of AC1NX476 with WT and their mutations.

**Figure S18** Correlation between the calculated binding free energy and (A) number of water molecules that have hydrogen bonds with AC1NX476, (B) number of water molecules having non-bonded contacts with AC1NX476, (C) number of residues forming hydrogen bonds with AC1NX476, (D) number of residues having non-bonded contacts with AC1NX476, and (E)volume of binding site of four receptors.